Tuning optical and electronic properties in novel carbazole photosensitizers for p-type dye-sensitized solar cells

(Article begins on next page)

02 August 2024

Corresponding Author: Professor Michele Pavone,

Corresponding Author's Institution: University of Naples Federico II

First Author: Antonio Carella

Order of Authors: Antonio Carella; Roberto Centore; Fabio Borbone; Maria
Toscanesi; Marco Trifuoggi; Federico Bella; Claudio Gerbaldi; Simone
Galliano; Eduardo Schiavo; Arianna Massaro; Ana Belen Muñoz-Garcia;
Michele Pavone

Manuscript Region of Origin: ITALY

Abstract: This work reports the synthesis and characterization of three
novel carbazole-based push-pull dyes that have been purposely designed to
be applied in p-type dye-sensitized solar cells (DSSCs). By using the
same electron-donor moiety (the carbazole group) and three different
electron acceptor groups (namely, X, Y, and Z), we explore how these new
substituents affect the optical and electrochemical properties of the
dye. State-of-the-art theoretical characterization at the DFT and TD-DFT
levels of theory provides the means to understand and elucidate the
connection between the chemical composition, the structure and the
electronic features of these dyes. The interface between the dyes and the
prototypical p-DSSC electrode (i.e. NiO) is also investigated by first-
principles calculations, highlighting the importance of taking into
account the dye/electrode mutual polarization for a correct alignment of
the relevant electronic states (e.g., dye HOMO and NiO valence band
edge). Following these characterizations, preliminary studies on the
photoelectrochemical performances of the new dyes in p-DSSCs provide
promising results and motivate future investigations on these new
systems.

*Response to Reviewers

Dear Editor,

We thank the three referees for their insightful analysis of our manuscript. We accepted their critics and we provide here an extensively revised manuscript that addresses all the reviewers' requests that were in our grasp.

Briefly, we rearranged the manuscript as suggested by reviewer 1, we improved our bibliography as requested by reviewer 2 and we addressed all the minor points of reviewer 3. The reviewers asked for a more extensive experimental characterization of the p-type cells. Unfortunately, we have not been able to access the experimental instrumentations that are needed to perform the requested experiments. For this reason, the revised manuscript gives much less emphasis to the p-type DSSC data that, at this point, must be further investigated in a future work.

However, despite the lack of advanced experiments on the DSSC performances, we hope that our work is still worth the publication on Electrochimica Acta thanks to the reported synthesis of new fully organic push-pull dyes, their experimental and theoretical characterization and the theoretical insights on the dye-electrode interface, together with the preliminary photoelectrochemical characterization of the performances of these dyes in p-type DSSCs.

Please find below our detailed point-by-point replies to the referees' comments and concerns.

Thank you very much for your kind consideration,

Michele Pavone

PS: Color legend, Reviewers' comments are in *blue italic*, our replies in normal text, the changes in the revised manuscript are <mark>highlighted in yellow</mark>.

Reviewers' comments:

Reviewer #1:

In this paper, new sensitizers are proposed for the sensitization of p-type NiO as semiconductor. The synthesis is presented in a very conclusive way and the calculations of molecular properties are performed on a high level and lead to reasonable conclusions. The molecular characterization by optical spectroscopy is performed and interpreted according to the state-of-the-art. This same statement still holds for the performance of the cyclic voltammetry measurements, but unfortunately not for their interpretation. The subsequent analysis of the photoelectrochemical performance is far below present state of the art and the results do not at all support the conclusions. The link to the calculations, therefore, is not possible. The calculations of molecules adsorbed to NiO albeit of general interest show some lack of relevance for the complex situation in a dye-sensitized solar cell. In the present arrangement the work can not be published. This reviewer just sees a chance to

rearrange the manuscript in a major revision effort to

A) synthesis of new molecules

B) DFT calculations on molecules

C) thermal, optical and cyclic voltammetry properties of molecules

D) DFT of Molecules adsorbed to NiO

We thank the reviewer, we have analyzed the comments below and we have modified the structure of the manuscript as suggested, but without the section E) because we do not have the access to the instrument that are needed to perform the requested experiments.

The following comments hopefully explain the above critical judgement and show why the present manuscript can not be published:

1) (page8) While eq. 1 and 2 can certainly serve to obtain a rough estimate of energy levels in molecules from cyclic voltammetry (CV) measurements they are far too shallow for a detailed interpretation of CV in an electrochemical journal. In this context, one would have to start with a discussion of chemical and thermodynamic reversibility. Both seem to be rather limited in the present cases. This would hinder one from determining a redox potential for either the reduction or oxidation of the molecules. The position of the onset of the respective reactions may then serve as an estimate (eq.1,2) but its limitation would have to be clearly stated. Further, it would have to be mentioned, how the reference was made to the ferrocene/ferrocenium (Fc/Fc+) couple. Presumably reversible waves were obtained in that case. Were the values of the molecules referred to the redox potential Fc/Fc+ or again to onset values?

We agree with the reviewer observation: we modified the text specifying that the CV measurements were meant to provide an internal comparison between the three dyes and to show how the different electron-acceptors used significantly influence the LUMO stability. We also provided more details about the way oxidation and reduction potentials were extrapolated by CV diagrams.

2) (page 10-11) The obtained cell efficiencies are referred to reported cells delivering about 0.05 %. Why not to the 2.5 % also reported? The quality of the NiO as electrode material was not independently proven. There is not even a reference provided that the NiO prepared according to the present procedure (page 23) is of sufficient quality. No characterization beyond the film thickness is provided. The amount of adsorbed dye is not specified. This amount, however, will directly be linked to the light harvesting efficiency of the respective cell. The whole discussion of dye efficiency in the manuscript, therefore, is obsolete since it is based on the implicit discussion of quantum efficiencies which are not at all accessible from the present data. There can be a number of reasons among sub-% cells why one cell performs a little better and the other a little worse. Further, statistics averaging over at least three replicas of cells for each dye would be needed. But even then it stays impossible to trace any (even if significant) differences back solely to the kinetics of light-induced hole injection as done by the authors. A complete cell characterization allowing to discuss differences in recombination, series resistance, CT-resistance at the counter electrode etc. would be needed to then perhaps extract differences in the injection kinetics which would then still include the regeneration step. Analysis of rate of tunneling (as used by the authors) during injection requires additional separate experiments with fs resolution. The correlation to calculated DFT data in conclusion is not possible based on the present experimental data.

We thank the referee for this comment, we have revised the discussion of photoectrochemical performance so to highlight the limits of our investigation that should be taken more as a preliminary proof-of-principle and will be subject to further studies.

3) (page 14 l.15) It is not clear to which "trend C1 to C3" is referred here. This problem persist on this page, e.g. "computed data", "experimental characterization", "photoelectrochemical characterization". The statement, that the theoretical model must be improved can not at all supported, because the experimental

In the revised manuscript we improved the description of the theoretical results by including also a further analysis on the effects of the molecular dipole to the hole-injection driving force.

4) (page 16) Calculations of relative density of states (DOS) in interfaces are certainly challenging and it is appreciated that the authors are facing this. The chosen model system already is quite complex as mentioned by the authors. It does still not include, however, components of the redox electrolyte which are decisive to surface energetics (traces of water, surface hydroxylates, electrolyte ingredients like ions adsorbed to the surface or in close proximity to the adsorbed molecules ...). So even if the authors had fully reliable photoelectrochemical cell data (which they do not have) the calculated values could not be used for a clear correlation. They could be used, however, to discuss results at model interfaces like molecules adsorbed to NiO, transferred to vacuum and then analyzed by photoelectron spectroscopy. Such experiments are needed to validate the calculations presented in Figure 7, photoelectrochemical cell data barely can serve this purpose. In turn, the calculated values can by no means be used to discuss the present solar cell data.

We agree with the referee that our model is just an ideal system without a lot of the features that are present in the real device. Nevertheless, fundamental knowledge can be also achieved by factorizing out the effects of the many p-DSSC components and by focusing on the intrinsic properties of the dye-electrode interface.

5) (page 16 /17) The discussion of electron (hole) transfer kinetics misses the main point of isoenergetic transfer, dictated by the Franck-Condon principle and implemented in the Marcus theory. The "driving force", therefore, is irrelevant   if a situation is known in such great detail as sketched in Figure 7. Rather the overlap integral of occupied states on the donor side (holes dye HOMO) and unoccupied state on the acceptor side (electrons VB NiO) are relevant. Both are calculated by the authors and provided in Figure 7 and looks similar for C1 and C3 but slightly smaller for C2. Of course this overlap could be nicely discussed by the authors. The rule of thumb considering the "driving force" is only needed if such detailed knowledge is missing and one has to consider the increasing DOS in the semiconductor away from the respective band edge.

Again, the referee is correct, but our objective was not to characterize the kinetics of hole injection, which would require much higher levels of theory, including the electronic excited states, that are not well described by DFT approaches based on super-cell surface slab models. Regarding Figure 7, there was an error in the scale of the C2 PDOS plot (the axis label was covering the axis tick labels) and it has been now fixed in the revised manuscript, all the three PDOS plots are similar and they don't present any difference concerning NiO states.

6) (page 17) Recombination in <1% cells will clearly be dominated by hole transfer from NiO to I- or by recombination of charges within NiO. The direct transfer of holes back to the reduced dye of course is also possible (but presumably represents a small part only). Again, more sophisticated experiments would be needed to elucidate this context rather than a more complex computational analysis as chosen by the authors. Further, the calculations would need to consider the SOMO of the reduced dye rather than the LUMO of the neutral molecule.

We agree with the referee and we will focus on this features in future experiments.

Minor aspects:

a) (Abstract, p.10) P1 is used as a reference dye without mentioning any scientific name.

In the revised abstract there is no longer the reference to the P1 and we now introduce the scientific names of the C1, C2 and C3 dyes in the new Scheme 1 caption.

b) (page 4) Sunlight is not ad- but absorbed.

Thanks for catching this typo, we have corrected this word in the new manuscript

c) (page5) Structural formula of C1-3 are missing. At least a hint to Figure 5 should be provided.

We inserted a new Scheme in the Introductory Section where the complete chemical structure of the compounds are reported

d) (page 6) The temperature (~245°C ?) of the endothermic phenomenon should be included to specify the signal the authors are thinking of.

We specified the required temperature value in the text.

e) (Figure 1) endo up reminds of lab slang rather than scientific units. It would be better to include a corresponding statement in the figure caption

Reviewer's suggestions were followed and the caption has been modified.

f) (Table 2) Eopt can not possible stem from electrochemical data. The label must have been confused with Eec. Each of these quantities should be systematically introduced in their origin and in their meaning.

In the revised manuscript the electrochemical and optical gaps were specified in their meaning and for what concerns their measurement.

g) (Figure 4) how was PCE normalized?

We thank the Referee for highlighting this typo, PCE values shown in Fig. 4 are not normalized data, but measured ones. It has been revised in the resubmitted manuscript.

h) (page 12) It needs to be specified what is meant by "first bright maximum absorption wavelength".

It was used as synonymous of "Vertical absorption wavelengths", which has been now better clarified in the new version of the manuscript.

i) (page 24) The size of the mask in cell illumination has to be adjusted to the cell area in order to avoid parasitic absorption by additional light scattering in the device (see doi.org/10.1002/pip.683). The "platinum carbon", "platinum wire", "Ag/AgCl" and "Fc/Fc+" could use some further specification of origin, purity and concentration.

We specified in the revised manuscript that the previously mentioned masked area (0.16 cm^2) is perfectly consistent with the electrode area (0.20 cm^2). This ratio is well in agreement with the good practice of DSSC measurements reported in several papers on experimental procedures for solar cells characterization, such as Energy Environ. Sci., 2013, 6, 54-66. Regarding the materials for CV measurements, we have added the required specifications in the experimental section.

Reviewer #2:

This paper reads well. By combined theoretical and experimental studies, three new dyes were developed for the sensitization of the p-NiO photocathode. The conclusions are sound and sufficiently supported. However, the manuscript requires some revision, which should address the comments listed below.

We thank the referee for the positive comments on our work.

Special points:

1. Update introductory references about DSC technology and electrochemical approach to their study by e.g.: Curr. Opinion Electrochem. 2, 88, 2017.

Thanks for pointing out this review that we have included in our revised reference section

2. What was the motivation for the DSC and TGA investigations? More importantly, the photochemical stability of novel dyes should have been addressed in addition to the thermal stability. Note that the reference dye for p-NiO sensitization (P1-dye) shows surprisingly fast degradation upon illumination in solution (PhysChemChemPhys 18, 16444, 2016).

We revised the discussion of the DSC and TGA investigation pointing out the new reference and the importance of the photostability of fully organic dyes as the P1.

3. The use of the dyes' redox potentials as a measure of HOMO/LUMO positions (Table 2) is questionable, if the redox potentials are determined in the electrolyte solution. The correct measurement must be carried out for dyes in the adsorbed state on the given semiconductor. Note that significant differences exist between the solution-potentials and, e.g. those of dye@TiO2 redox couples (ChemSusChem 11, 494, 2018). Similar experiment using p-NiO would be important.

We agree with the reviewer observation: we modified the text specifying that the CV measurements were meant to provide an internal comparison between the three dyes and to show how the different electron-acceptor used significantly influence the LUMO stability. Unfortunately, with our current set-up we are no able to perform CV measurement using a sensitized NiO working electrode: once again, we agree with the referee that such a measure would be ideal for DSSC applications.

4. CV is not a 'spectrum' (Fig 3). Also the current scale should be labelled on the picture and the caption should be more descriptive (scan rate and direction, electrolyte solution, etc.)

We perfectly agree and corrected our error.

5. The aging-induced enhancement of PCE is interesting. It would be helpful to see the IPCE spectra of fresh and aged devices to account for possible structural changes in addition to the speculation about 'wetting' of the electrode.

We thank the Referee for the interesting suggestion. Even if we do not have the lab equipment to carry out IPCE measurements (especially with a sensitivity high enough to detect the small photocurrent that can be

generated by p-type cells), we initially excluded this effect from our hypotheses due to the fact that Jsc values (listed in Table 3) measured on 1st and 50th did not show significant variation upon aging. Conversely, we observed increased V_{oc} and, sometimes, FF values. Even if these parameters can be influenced by several parameters, we attributed their variation to electrode wetting and permeation by the electrolyte. Indeed, based on our previous experiences, the commercial electrolyte Iodolyte Z-150 takes some time to reach the maximum efficiency when injected in solar cells. Indeed, its formulation is conceived for high-stability cells, and it is prepared with nitrile solvents more viscous than acetonitrile.

Anyway, as stated above, photoelectrochemical performance were carried out here as proof-of-principle for the operation of proposed dyes and will be subject to further studies.

We thank the reviewer for the positive comments on our work, as for the reviewer 1 the requested additional experiments are not within our grasp and we have revised the structure of the paper by pointing also out the needs of further experiments to rationalize the reported preliminary results on PEC performances.

Agreed, we updated the text in the revised manuscript.

Thanks again, we have corrected the text.

* Also on p4 the authors discuss the limitations of using NiO and I-/I3- in terms of device Voc, yet fail to mention that the 2.5% attained was done using a Co(2/3+) complex. Using such a mediator however impacts upon the attainable voltage on the photoanode side in a tandem device (the ultimate aim). I think a little bit of extra explanation would benefit the less specialized reader (while the specialized reader will already know all of this).

Thanks for pointing this out, we have corrected the text accordingly.

* on p9 the authors write "the HOMO energy, instead, is not much influenced...". Perhaps something like "The HOMO energy is not strongly influenced..." could be used.

Corrected

* on p10 the authors refer to the "relative" photoelectrochemcial parameters. I suspect they mean "relevant" or "respective"?

Corrected.

* Can the authors explain the large discrepancy (~0.6-0.9 eV) in experimentally determined versus calculated LUMO energies?

The experimental LUMO values are derived by experiments in DCM while computed ones are obtained in acetonitrile solution. Moreover, the electrochemical derived LUMO includes also the electronic reorganization energy for the reduction of the dye, while computed LUMO values are obtained for the unperturbed neutral dye. We have pointed this out in the revised manuscript.

* Given the comparatively small shift in electron densities between HOMO and LUMO, did the authors look at other orbitals which may be involved (such as LUMO+1)?

Yes we have analyzed all the MOs of the dyes, but the relevant ones for the most bright electronic transition are only the HOMO and LUMO.

* The stability data presented is impressive, however it would be interesting to see this presented alongside other dyes (P1 / C343 are two examples that come to mind).

This is a good idea, but we have postposed further PEC experiments to a future work.

* In the interest of full disclosure, the authors should probably state that their method of introducing p-type character through the removal of an Ni atom is actually around a million times more heavily doped than in a real system.

That is true, we have clarified this point in the Computational Details section

* When discussing driving forces for hole injection, it would be good to compare against other highly efficient pDSC systems with reported values

Thanks for this good idea, it is actually difficult to find results that are comparable to those obtained in this work because there are only few works that addressed the modeling of dye-electrode interface in p-DSSCs.

* I assume the short names of the compounds reported under dye synthesis are not supposed to have a subscript (p20-22)?

Corrected

* TBAPF6 is not an 'inert' electrolyte, but rather a non-redox active one

It is true and we corrected in the text accordingly

Tuning optical and electronic properties in novel carbazole photosensitizers for p-type dye-sensitized solar cells

Antonio Carella,[a,*] Roberto Centore,[a] Fabio Borbone,[a] Maria Toscanesi,[a] Marco Trifuoggi,[a] Federico Bella,[b] Claudio Gerbaldi,[b] Simone Galliano,[c] Eduardo Schiavo,[a] Arianna Massaro,[a] Ana B. Muñoz-García,[d] and Michele Pavone[a,*]

a) Department of Chemical Sciences, Università di Napoli Federico II, Comp. Univ. M. Sant'Angelo Via Cintia 21, 80126 - Napoli, Italy

b) GAME Lab, Department of Applied Science and Technology - DISAT, Politecnico di Torino, Corso Duca degli Abruzzi 24, 10129 - Torino, Italy

c) Department of Chemistry, NIS Interdepartmental Centre and INSTM Reference Centre, Università degli Studi di Torino, Via Pietro Giuria 7, 10125 - Torino, Italy

d) Department of Physics "Ettore Pancini", Università di Napoli Federico II, Comp. Univ. M. Sant'Angelo Via Cintia 21, 80126 - Napoli, Italy

* Corresponding authors:

A.C. antonio.carella@unina.it; TEL: +39 081 674446; FAX: +39 081 674090

M.P. michele.pavone@unina.it; TEL: +39 081 674210; FAX +39 081 674090

ABSTRACT

This work reports the synthesis and characterization of three novel carbazole-based push-pull dyes that have been purposely designed to be applied in p-type dye-sensitized solar cells (DSSCs). By using the same electron-donor moiety (the carbazole group) and three different electron acceptor groups (namely, X, Y, and Z), we explore how these new substituents affect the optical and electrochemical properties of the dye. State-of-the-art theoretical characterization at the DFT and TD-DFT levels of theory provides the means to understand and elucidate the connection between the chemical composition, the structure and the electronic features of these dyes. The interface between the dyes and the prototypical p-DSSC electrode (i.e. NiO) is also investigated by first-principles calculations, highlighting the importance of taking into account the dye/electrode mutual polarization for a correct alignment of the relevant electronic states (e.g., dye HOMO and NiO valence band edge). Following these characterizations, preliminary studies on the photoelectrochemical performances of the new dyes in p-DSSCs provide promising results and motivate future investigations on these new systems.

1. INTRODUCTION

The worldwide concerns on exploitation of fossil fuels and the corresponding environmental issues have motivated an intense research activity toward the development and implementation of sustainable technologies for energy conversion and storage, from fuel cells to Li-ion batteries [1-2], from wind-power plants to photovoltaic panels [3]. In particular, sunlight represents the most convenient renewable energy source on earth, but an effective deployment of photovoltaics is still hindered by the technological challenges of achieving an efficient conversion with cheap materials. In this context, solid-state silicon-based solar panels are the current workhorse devices for solar energy conversion, but still provide low efficiency in diffuse light conditions (cloudy days). Moreover, production and maintenance costs are still higher with respect to other solar technologies [4]. Thus, research efforts have been focusing on novel devices based on the alternative paradigm of solar energy conversion relying on photo-electrochemical processes for electron-hole separation and charge carrier diffusion across heterogeneous organic-inorganic interfaces [5].

The seminal paper of Grätzel and O'Regan [6] has opened the field of dye-sensitized solar cell (DSSC) technology as cheap and efficient alternative to solid-state solar panels [7]. More recently, great attention has shifted from DSSCs to perovskite solar cells [8] and new technologies based on organic materials [9] or hybrid systems [10]. Despite the high efficiency records, these new technologies present problems of long-term stability [11]. Hence, DSSC technology has many appealing features and still retains an important role in the photovoltaics scenario. Recently, new electrolyte complexes have allowed record photo-conversion efficiency (PCE) beyond 14% [12] and, more recently, completely water-based systems have been demonstrated as efficient replacement of toxic organic solvents, thus accounting for truly sustainable devices [13]. The transparency and the possibility of applying different coloured dyes can allow the integration of DSSC in architectural elements in energy-efficient building [14], and last but not least the optical properties of the dye can be purposely tuned to achieve up to ~25% efficiencies in recycling indoor light [15].

Further developments of DSSCs may be achieved by the implementation of tandem cells, where the standard cell based on a dye-sensitized n-type semiconductor oxide, the photo-anode, is coupled to a DSSC working as photocathode with a p-type semiconductor oxide [16,17]. Such set up can achieve in principle a photo-conversion efficiency of ~40% [18,19]. So far, the deployment of tandem cells based on DSSCs has been hindered by the extremely low efficiencies of p-type devices [20, 21]. The limited p-type DSSC conversion performances are to be mostly ascribed to the use of nickel oxide as p-type semiconductor [22]. For example, the position of p-NiO valence band edge is too high in energy; hence, its proximity to the electrolyte redox potential (e.g. I^-/I_3^-, Co^{2+}/Co^{3+} complexes) limits the open circuit potential (V_{oc}) [23]. Though, the position of the redox potential of the electrolyte is only relevant in single (p- or n- type) devices. When these are connected into a tandem cell, the V_{oc} will only depend on the difference between the conduction and valence bands of the photoanode and photocathode, respectively. The low NiO dielectric constant determines a strong interaction between hole and electrons, thus leading to easy charge recombination [24]. Nevertheless, the sensitizing dye can also play an important role in the cell performances [25-29], the key parameters are: a good absorption of sunlight (i.e. high molar extinction coefficient) and an intra-molecular charge transfer upon photoexcitation, so that the electron is localized far from the electrode surface and the hole is localized close to the anchoring group. The design of new dyes with such characteristics is highly desirable, but it may be not sufficient, because the interfacial electronic features can still hinder the dye regeneration/hole injection processes that lead to the photocurrent generation.

To address these two crucial aspects in p-type DSSCs, i.e. molecular dye properties and interfacial electronic features, we performed a combined experimental and theoretical study on three new, purposely synthesized push-pull organic dyes, based on a carbazole electron-donor moiety functionalized with an anchoring group, on one side, and with three electron acceptor groups of different electron withdrawing strengths, on the other. The chemical structures of the synthesized dyes are shown in Scheme 1.
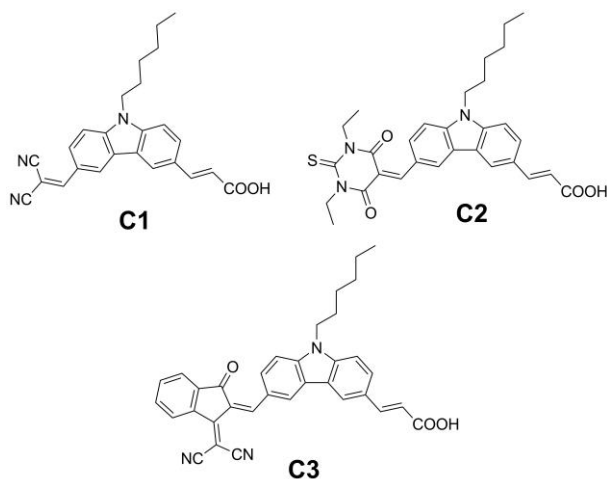
Scheme 1. Chemical structures of the synthesized dyes: (E)-3-(6-(2,2-dicyanovinyl)-9-hexyl-9H-carbazol-3-yl)acrylic acid (**C1**), (E)-3-(6-((1,3-diethyl-4,6-dioxo-2-thioxotetrahydropyrimidin-5(2H)-ylidene)methyl)-9-hexyl-9H-carbazol-3-yl)acrylic acid (**C2**), (E)-3-(6-((Z)-(1-(dicyanomethylene)-3-oxo-1H-inden-2(3H)-ylidene)methyl)-9-hexyl-9H-carbazol-3-yl)acrylic acid (**C3**).

For each of these dyes, we characterized the optical and electrochemical properties in solution. The experimental results are rationalized by means of state-of-the-art ab initio calculations based on density functional theory (DFT) [30-31] and time-dependent DFT (TD-DFT) [32], including the effects of the solvent via the polarizable continuum model (PCM) of implicit solvation [33], and by addressing the dye-electrode interfacial properties with a periodic slab approach, as recently proposed for the C343/NiO interface [34]. In particular, this interface between the C1, C2 and C3 dyes and the prototypical p-DSSC electrode (i.e. p-NiO) highlights the importance of taking into account the mutual dye-electrode polarization for assessing a correct alignment of the dye HOMO and the p-NiO valence band edge, which are the relevant electronic states for the hole injection process after photo-oxidation of the dye [34].

Following these characterizations, preliminary studies on the photoelectrochemical performances of the new dyes in a standard p-DSSC set-up under simulated solar radiation provide the first promising PCE performances that are comparable to those obtained with other push-pull dyes. Thus, our results motivate future investigations on these new systems for a full characterization of their photoelectrochemical properties within the p-DSSC devices.

2. RESULTS AND DISCUSSION

2.1 Dye synthesis and characterization

The new dyes are based on a carbazole electron-donor moiety, functionalized with an acrylic acid end group for anchoring to the nickel oxide electrode in the p-DSSC assembly. The carbazole molecular motif, common to the three dyes, has been then functionalized with electron acceptor groups of different strength with the aim of tuning optical and electronic features, as reported in previous papers [35-39]. The dyes have been synthesized through a multistep procedure as shown in Scheme 2.
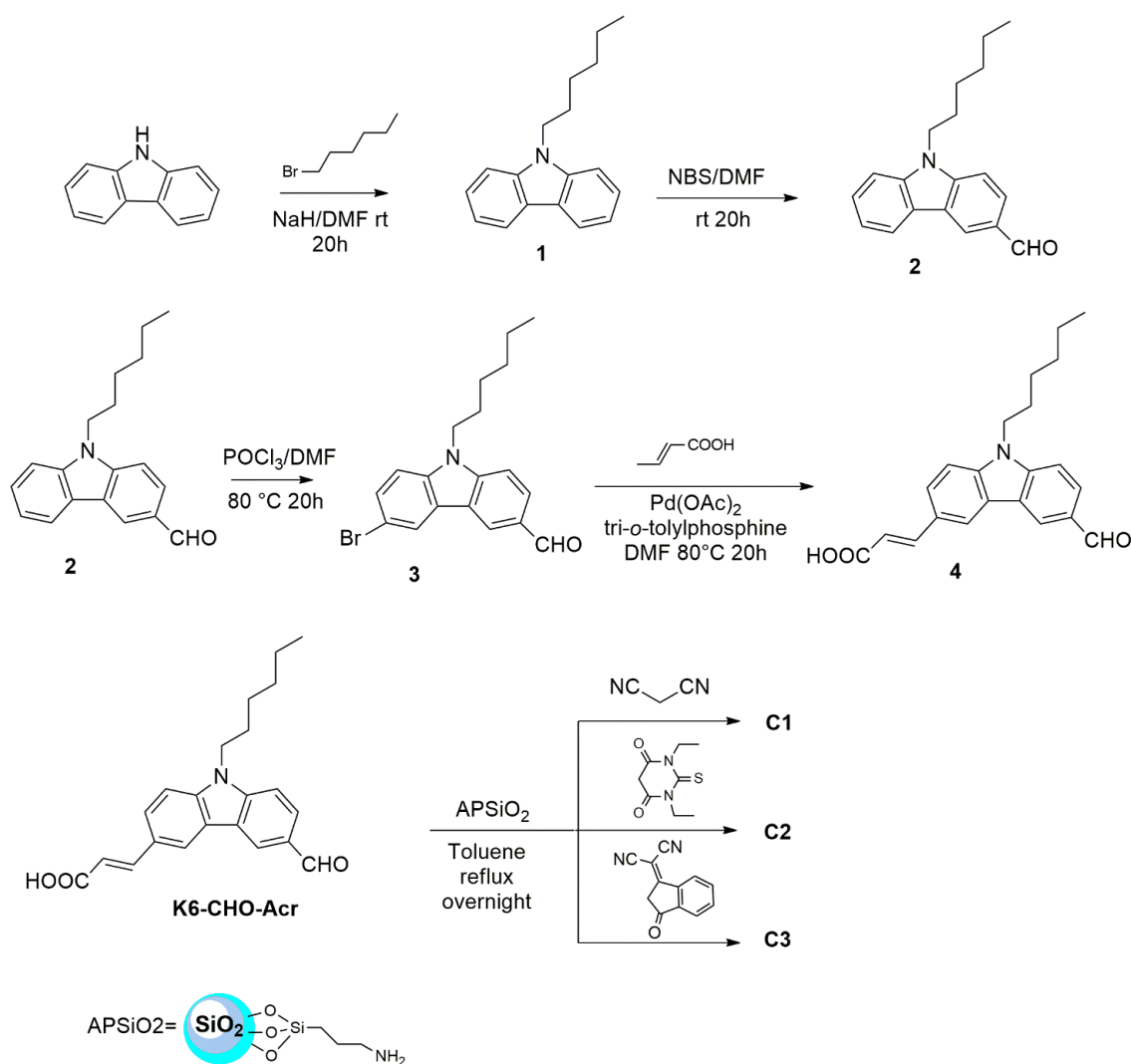

Scheme 2. Synthetic pathway for the dyes under study.

Carbazole has been functionalized with a solubilizing hexyl chain by reaction with bromo-hexane in dimethylformamide (DMF) in presence of sodium hydride. The so obtained alkylated compound (**1**)

has been formylated in position 3 by a Vilsmeyer-Haack reaction (**2**) and then brominated in position 6 in a reaction with bromine (compound **3**). A carboxylic group has been then introduced in the molecular backbone by reacting compound **3** with acrylic acid in a palladium catalysed Heck reaction. This aldehydic precursor (compound **4**) has been used to synthesize the three reported dyes in a Knoevenagel reaction with three different electron acceptor systems as malononitrile, thiobarbituric acid and a dicyanovinyl-functionalized indandione derivative. The Knoevenagel condensation is a well-known C-C bond formation reaction occurring between aldehydes or ketones and compounds containing active methylene groups. The reaction is usually performed in organic solvents and is typically catalysed by ammonia or primary or secondary amines as piperidine [40,41]. A great variety of other catalytic systems have been anyway reported [42-44]: in particular, silica bearing amino functionalities (aminopropyl functionalized silica) is reported as an efficient catalyst for this kind of reactions [45,46] and has been used in the synthesis of the three dyes under study. The reaction has been performed in toluene at reflux overnight and the dyes were obtained in good yields, ranging from 65 to 74%.

Phase behaviour of the three dyes has been investigated via DSC analysis. As shown in Figure 1, the three dyes are characterized by sharp endothermic peaks, corresponding to the melting of the compounds. Melting temperatures (listed in Table 1) are, respectively, 242, 263 and 278 °C for **C1**, **C2** and **C3**. This trend is presumably influenced by two factors: the increase of molecular weights and the increased strength of dipolar interactions, which are higher in the system bearing the stronger electron withdrawing group (**C3**). For what concerns DSC trace of **C3** it is possible to observe an endothermic phenomenon prior the melting, centred at 245 °C and associable to a solid-solid transition. Just after melting **C3** experiences an exothermic peak associable to thermal decomposition.
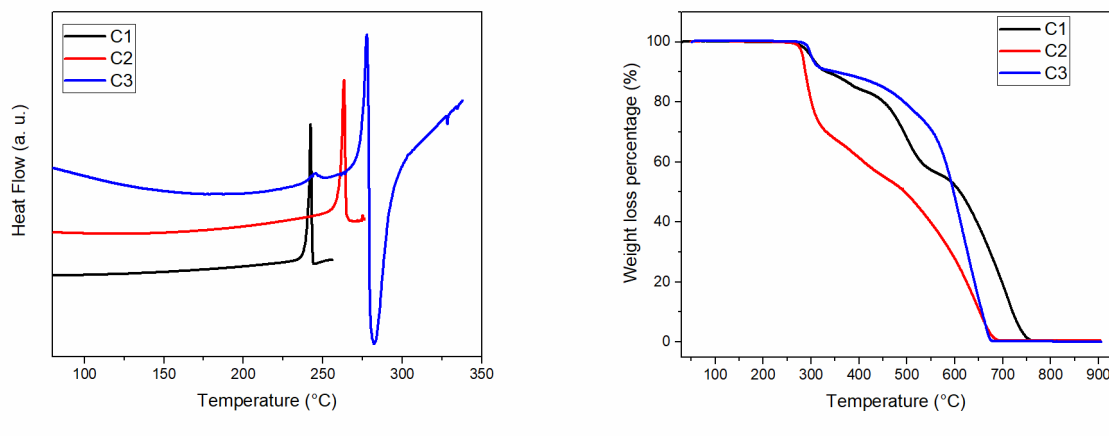
Figure 1. (A) DSC traces and (B) TGA plots for **C1**, **C2** and **C3**. In DSC plot endothermic flux is directed upwards.

The thermogravimetric (TGA) analysis has been performed to investigate thermal stability of the dyes and it is also reported in Figure 1. The dyes are characterized by a fair good thermal stability with decomposition temperatures (defined as the temperature corresponding to the weight loss of 5%) between 283 and 301 °C (see Table 1). The DSC and TGA investigation were motivated by the concern regarding full organic dyes that have shown very low thermal stability, which can compromise the long-term performance of the p-DSSCs [47].

All the dyes have been characterized by UV-Vis spectroscopy in tetrahydrofuran solution; the optical spectra are reported in Figure 2. Qualitatively, the three sensitizers present two principal optical features, one occurring in the UV and the other in the visible part of the spectrum. The strength of the electron acceptor group used has a clear influence on the dye absorption properties. In particular, the higher is the electron acceptor ability the more red-shifted is the wavelength of the absorption maxima. The three dyes **C1 C2** and **C3** present absorption maxima at 411, 465 and 514 nm, respectively, thus covering a significant part of the visible spectrum. Quantitatively, the three novel compounds are characterized by a fair high molar extinction coefficient, ranging from 35000 $cm^{-1} M^{-1}$ to 44000 $cm^{-1} M^{-1}$. The optical properties of the dyes are reported in Table 1.

Table 1. Thermal and optical properties of the synthesized dyes.

	T_m (°C)[a]	T_d (°C)[b]	λ_{max} (nm)[c]	ε (cm^{-1} M^{-1})[c]	λ_{max} (nm)[c]	ε (cm^{-1} M^{-1})[c]
C1	242	301	297	4.04·10^4	411	3.54·10^4
C2	263	283	300	4.44·10^4	465	4.44·10^4
C3	278	301	302	5.03·10^4	515	3.71·10^4

[a] Measured by DSC analysis in nitrogen atmosphere at a scan rate of 10°C min^{-1}.

[b] Corresponds to a weight loss of 5% as determined by TGA analysis performed in air atmosphere at 20 °C min^{-1}.

[c] Measured by UV-Vis absorption analysis in THF solution.
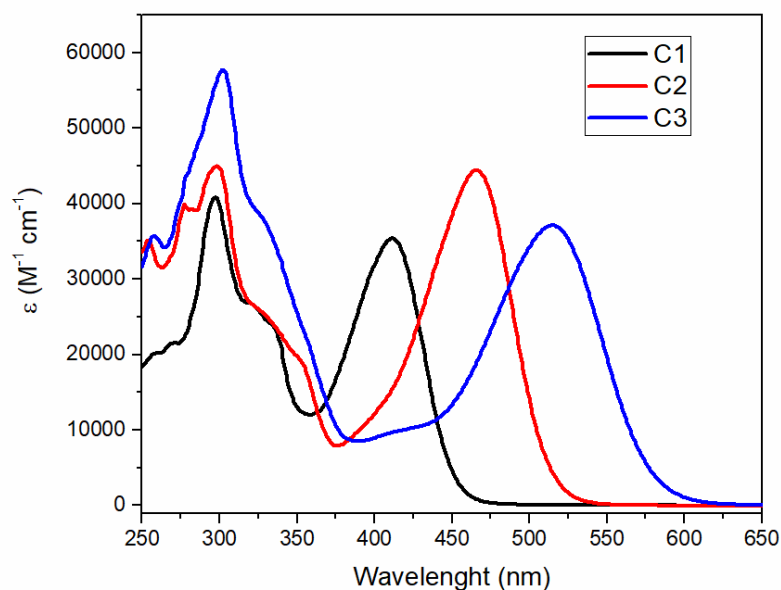
Figure 2. Molar absorptivity of the reported dyes in THF solution.

Oxidation and reduction potentials of the dyes have been measured by means of cyclic voltammetry and standardized versus the ferrocene/ferrocenium redox couple (Fe/Fe$^+$). The onset value of both oxidation and reduction peaks have been considered while, for what concerned ferrocene, the oxidation half-wave potential has been used. The CV plots are shown in Figure 3.
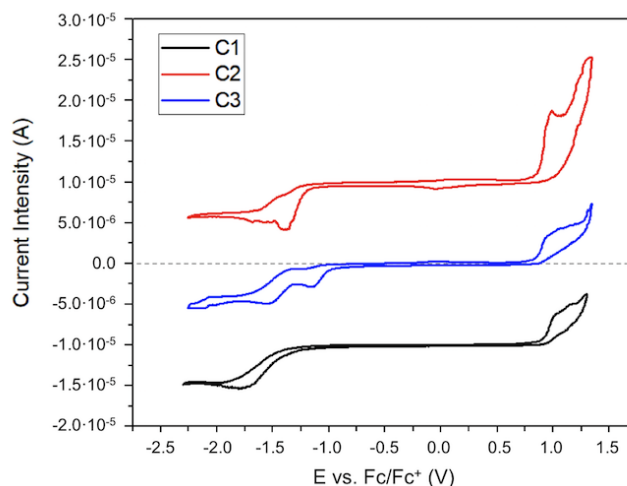
The oxidation and reduction potentials can be correlated, respectively, to the HOMO and LUMO energies of the dyes, according to the following formula [48]:

$$E_{HOMO} = - (E_{onset, ox} - E_{Fc/Fc}{}^{+} + 5.1) \tag{1}$$

$$E_{LUMO} = - (E_{onset, red} - E_{Fc/Fc}{}^{+} + 5.1) \tag{2}$$

The so-computed HOMO and LUMO energies refer to the dyes in solution and cannot exactly represent the real situation during p-DSSC operation, where dyes are adsorbed on NiO and immersed in a different electrolyte solution. Here we use these values with the objective of comparing the three dyes and for highlighting the effects of the different functionalization on a same molecular fragment. In particular, we found that the strength of the electron withdrawing group has a marked influence on the dye LUMO energies: as the strength of this group increases the LUMO stability of the corresponding dye increases. The HOMO energy, instead, is not significantly influenced by the electron acceptor group, resulting only slightly destabilized as the electron withdrawing strength increases. Thus, the stabilization effect of the LUMO by the electron acceptor group drives the modulation of the dye optical absorption properties. The further details

on the nature of the frontier orbitals and the electronic structure of the dyes are discussed in the following section. The dyes electrochemical properties are listed in Table 2 together with the electrochemical gap (E_{EC}), measured as the difference between the computed LUMO and HOMO energies: consistently with the optical gap (E_{OPT}) values determined by UV/Vis measurements in THF solution, E_{EC} decrease as the strength of the electron acceptor group increases.

Table 2. Electrochemical properties of the synthesized dyes.

	$E_{ox}(V)$[a]	$E_{red}(V)$[a]	$E_{ec}(eV)$[b]	$E_{opt}(eV)$[c]	E_{HOMO} (eV)	E_{LUMO} (eV)
C1	0.92	-1.37	2.29	2.69	-6.02	-3.73
C2	0.89	-1.22	2.11	2.35	-5.99	-3.88
C3	0.84	-0.99	1.83	2.07	-5.94	-4.11

[a] the potentials refer to the onset of the oxidation and reduction process; they have been measured vs the oxidation potential of ferrocene/ferrocenium couple in dichloromethane solution (≈0.3 mM); [b] determined by CV measurements as the difference between the onset of oxidation and reduction potentials; [c] determined by optical measurements in THF solution.

2.2 Theoretical analysis

In order to rationalize the different optical and electrochemical properties of the dyes, we have first performed a complete characterization of the dye structural and electronic features at the DFT and TD-DFT levels of theory. We have carried out the structural optimizations of the **C1**, **C2** and **C3** dyes in acetonitrile, but to simplify the calculations we replaced in our model the long alkyl chain by a simple methyl group, because the alkyl chain does not affect the electronic features. Acetonitrile (ACN) has been selected because it is the common solvent used in p-DSSC devices. For all the dyes, we considered different conformations of the electron-acceptor groups with respect to the carbazole moiety, but no significant differences in energy were found. The minimum-energy structures of all the three dyes are shown in Figure 5, together with the HOMO and LUMO isodensity surface plots.
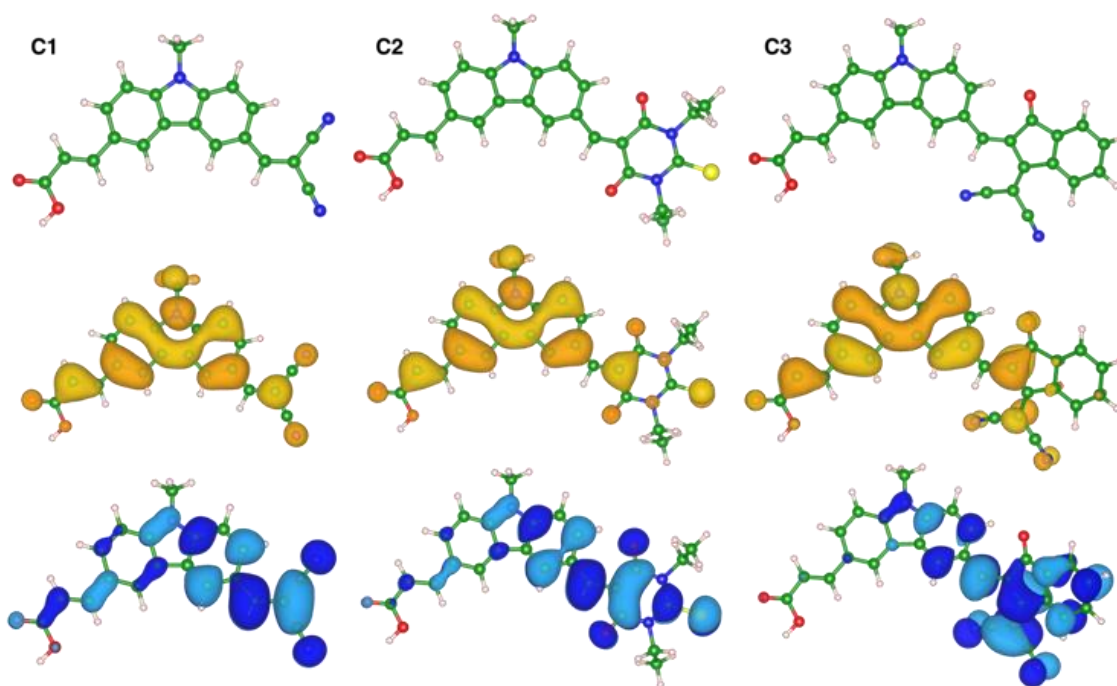
Figure 5. Minimum-energy structures of **C1**, **C2** and **C3** model dyes in ACN (top panel), HOMO (middle) and LUMO (bottom) (isodensity surface level: 0.02 a.u.; positive/negative surfaces are in yellow/orange and blue/cyan for HOMO and LUMO, respectively). Color legend: C green, O red, Ni blue, S yellow, and H white.

From qualitative analysis of the frontier molecular orbitals, in all the three dyes the HOMO is well localized on the carbazole moiety, and as expected the LUMO is mostly involving the electron acceptor groups. The degree of LUMO localization on these groups is consistent with the expected electron-withdrawing strength going from **C1** to **C3**. On these minimum-energy structures, we have performed TD-DFT calculations to characterize the dye optical properties. The overall good overlap between the HOMO and the LUMO allows for a good vertical excitation absorption of the incident light, as proven by the high oscillator strength values that correspond to the HOMO-LUMO transition. The vertical absorption maximum wavelengths and the corresponding oscillator strengths are listed in Table 4 for the three dyes.

Table 4. Computed electronic properties of the **C1**, **C2** and **C3** dyes. Vertical absorption wavelengths (λ_{max}) and corresponding oscillator strengths (f), E_{0-0} transition energy (see text), and absolute energy position of HOMO and LUMO. All the data have been computed in ACN.

	λ_{max}(nm)[a]	f	E_{0-0} (eV)	E_{HOMO}(eV)	E_{LUMO} (eV)
C1	361	1.347	3.10	-6.06	-2.96
C2	389	1.626	2.75	-6.00	-3.25
C3	425	1.165	2.57	-5.85	-3.28

[a] Absorption wavelength for the HOMO-LUMO vertical transition.

The TD-DFT results (computed in ACN) are in qualitative agreement with the experiments (carried out in THF). The observed discrepancies between measured and computed LUMO energies are mainly due to the different solvents employed. Moreover, the electrochemically derived LUMO includes also the reorganization energies for the reduction of the dyes, which are not present in the computed one. The observed visible band maxima (411, 465, 514 nm for **C1**, **C2** and **C3**) present the same trend of computed values, with a red shift of the band going from **C1** to **C3**, with **C2** presenting the maximum value of the oscillator strength, in agreement with the experimental maximum value of the molar extinction coefficient among the dyes. Analysis of the TD-DFT transition shows that this first bright band corresponds to the vertical transition from the HOMO to the LUMO, as expected. Table 4 lists also the data relative to the E_{0-0} transition for each dye, i.e. the energy difference between the S^1 excited state minimum energy structure and the S^0 ground state. This transition, together with the HOMO energy values from ground state calculations, allowed us to evaluate the absolute energy position of the LUMO to be compared with the electrochemical data reported in Table 2: the theoretical results present again the same trend as the experimental counterparts.

Another key property of the dye is the intramolecular charge-transfer (ICT) upon photoexcitation. Following the approach proposed by Ciofini and co-workers [49], we have quantified the extent of this ICT by analysing the electron densities of the ground and the excited electronic states: we

have thus determined the charge transfer excitation length (D_{CT}) and the transferred amount of charge (q_{CT}), the corresponding results are listed in Table 5.

Table 5. Intramolecular charge-transfer parameters upon photoexcitations: distance of the charge transfer (D_{CT}) and amount of electronic density that is transferred (q_{CT}) [49].

	D_{CT}(Å)	q_{CT}(e⁻)
C1	2.65	0.601
C2	2.83	0.642
C3	3.45	0.694

The analysis of the ICT results shows that the distance of the charge transfer and the amount of charge displaced upon photoexcitation follow the expected trend from **C1** to **C3**. If we consider the molecular properties of the dye in solution, the computed data are in good agreement with the experimental characterization. From the optical properties and the extent of the ICT the expected trend in relative PCE for the three dyes is **C3** > **C2** > **C1**. However, DSSC are complex multicomponent devices where the interfaces between different materials play a crucial role, so the analysis of the molecular properties alone might not be sufficient to draw reliable conclusions. Here, we have carried out an analysis of the interface between the **C1**-**C3** dyes and the nickel oxide electrode surface. NiO is the most employed p-type semiconductor in DSSC, even though it has some major flaws that limit pDSSC efficiency. In our surface model, we used a 5-layer slab of the NiO (100) surface, we removed a neutral Ni atom from the central layer, so to introduce holes in the system in order to account for the p-type character of the NiO used in the real devices. We must note that this choice introduce a hole concentration in our model that is higher than the commonly employed p-NiO electrode, but the same model provided good qualitative results for the C343/NiO(100) interface [34]. Also, our dye-electrode interface model is obviously still far from the complexity of the real system, where several other species take part in complex surface equilibria. Still, the advantage of computational modelling comes from the possibility to factorize out the system, rationalizing the different contributions.

These calculations were carried out with periodic boundary conditions (PBC) at the PBE+U level of theory, using the VASP code (see below for computational details). Figure 6 shows the minimum-energy geometries of the dyes adsorbed on the p-type NiO. Only the dyes and the two surface topmost layers were relaxed, while the bottom layers were kept frozen at the bulk position.
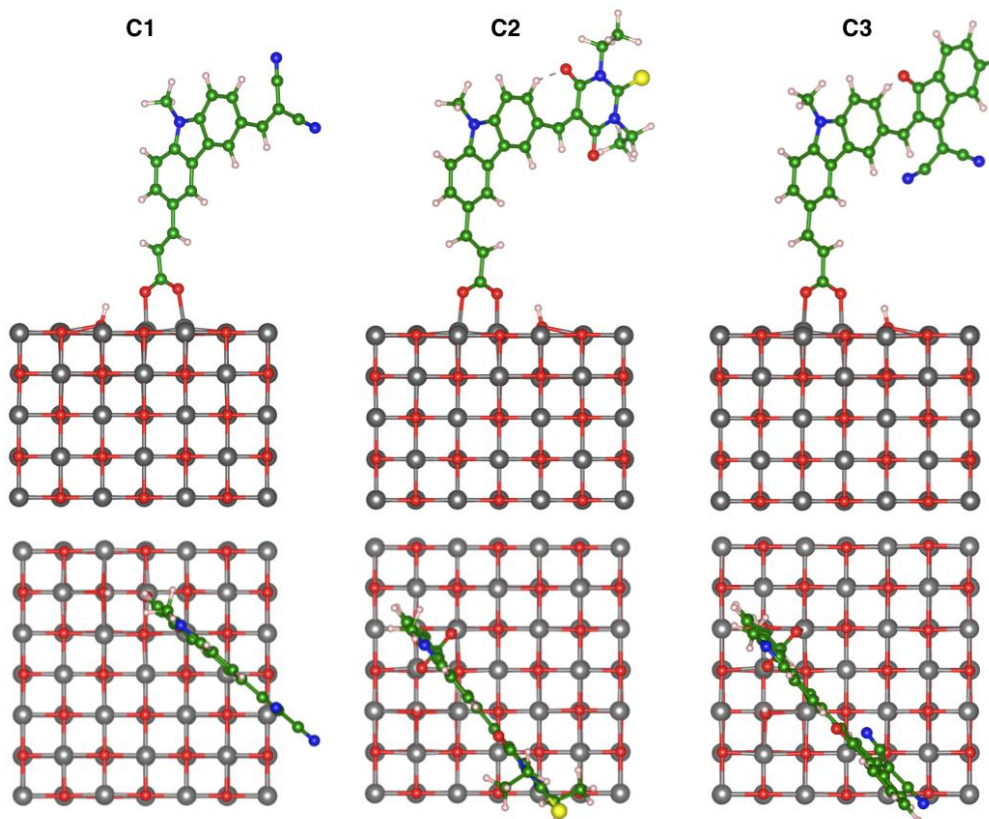

Figure 6. Dyes anchored on the 5-layer p-type NiO surface slab, side view (top) and top view (bottom). All the dyes are anchored through the carboxylate group in a bidentate configuration. Colour legend: C green, O red, Ni grey, N blue, H white, S yellow.

All the dyes have been anchored on the NiO surface with the same bidentate binding mode that is the most stable for the carboxylic acid-based anchoring group [34]. The oxygen atoms of the carboxylate group are bound to two different Ni atoms, while the proton is bound to NiO surface oxygen. The dyes are mostly planar, and this plane lies perpendicular to the NiO surface. After relaxation in vacuum, we have performed single-point calculations to include the effects of the acetonitrile solvent medium with the implicit solvation model implemented in VASP. From these calculations on the electronic properties of the dye-NiO interface in solution, we can compute the

thermodynamic driving force for the hole injection from the photo-oxidized dye to the electrode surface. An estimate of such driving force is the energy difference between the p-type electrode (i.e. NiO) Fermi level, considered as the topmost occupied states of the valence band (VB), and the HOMO of the adsorbed dye. These data for the three **C1**-**C3**/p-NiO systems can be obtained by the analysis of the interfacial electronic features, as for example the atom- and angular-momentum projected density of states reported in Figure 7.
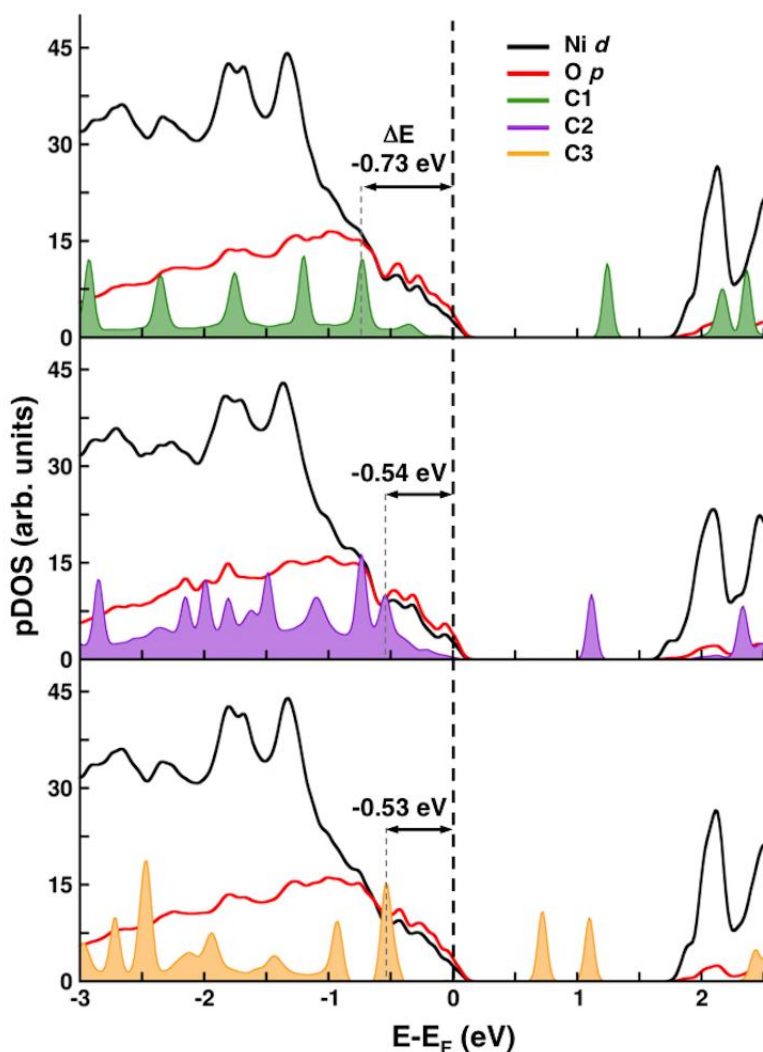
Figure 7. Atom- and angular-momentum projected density of states of **C1** (top) **C2** (middle) and **C3** (bottom) adsorbed on NiO. Colour code is displayed in the legend in the upper right corner. The Fermi energy (E_F) set to zero. Solid black arrows indicate the distance from the last populated peak of the molecules and the Fermi level (i.e. the ΔE for hole injection).

From analysis of these plots, in all the cases the Fermi level crosses the valence band of NiO, as expected for a p-type semiconductor. The hole injection driving force is computed as $\Delta E = E_{HOMO} - E_F$, as follows from an electron transfer from the VB to the dye HOMO. These values correspond to thermodynamic driving forces that do not take into account the kinetic parameters of the actual charge transfer process. However the so-computed ΔE has been widely accepted as a good approximation and provides valuable information when comparing different dyes [5,34]. **C2** and **C3** present very similar ΔE values, while the hole-injection driving force for the **C1** is significantly more convenient than the other two, -0.73 eV versus ~-0.54, i.e. an improvement of ~35%. A large driving force corresponds to a more efficient hole injection [5] that is crucial to obtain high PCEs, since the J_{sc} is directly dependent on this parameter. Here, the best choice seems to be **C1**. Thus, the expected trend in PCE efficiencies should be **C1** > **C2** = **C3**.

On the other side, charge recombination processes involve the charge transfer from the photo-excited dye (i.e. the dye LUMO) to the electrode (i.e. the p-NiO VB edge). These recombination competes with hole injection and it is the main responsible for the overall efficiency loss of the p-NiO based DSSC cells. A thorough analysis of kinetics and thermodynamics of this process would require a more complex computational analysis and is beyond the purpose of this work. However, it has been observed, both experimentally [50] and computationally [51], that the rate of recombination strongly depends on the distance between the excited electron localization (the LUMO of the dye) and the surface of the electrode. Figure 8 shows, for each dye, the projected density of the first unoccupied band of the dye-electrode interface.
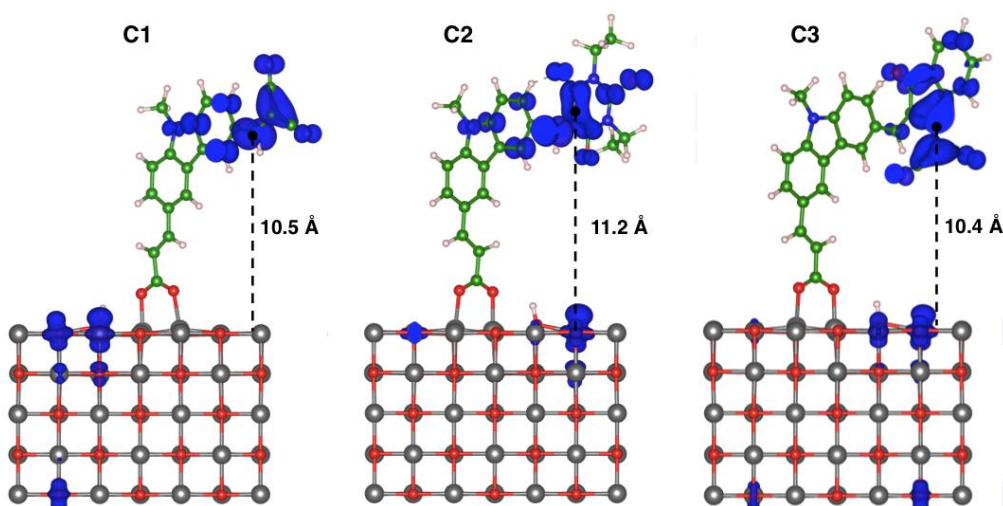
Figure 8. Distance between the surface of NiO and the centroid of the dye LUMO, defined as in ref. 50 (in the image the isodensity surface level is set to 0.0025 a.u.). Colour legend as in Fig. 6.

These isodensity surface plots correspond to the dye LUMOs that are strongly localized on the electron acceptor groups in all the cases. From these data we can qualitatively measure the distance between the electron and the p-NiO surface by considering the centroid of this isosurface plot, thus providing an estimate of how likely the charge recombination process can occur. The results are very similar for all the three dyes and we can conclude that all the three dyes have similar probabilities to undergo the unfavourable charge-recombination process.

2.3 Preliminary study on p-DSSC devices based on C1, C2 and C3 dyes.

After the synthesis and characterization of the new dyes and the theoretical analysis of their electronic structure and dye-electrode electronic features, we present here a first proof-of-principle study on the feasibility of these dyes in real p-DSSC devices. Thus, **C1**-, **C2**- and **C3**-sensitized NiO electrodes have been employed as photocathodes in p-type DSSCs. J-V curves and the corresponding photoelectrochemical parameters (short-circuit current density: J_{sc}; open-circuit potential: V_{oc}; fill factor: FF; power conversion efficiency: PCE) are shown in **Figure 4** and Table 3, respectively. The PCE values are low but consistent with state-of-the-art p-type DSSC devices with similar electrode preparation and the reference **P1** dye (PCE ~0.05%) [52,53], and other carbazole

based dyes (PCE ~0.04%) [54]. It clearly emerges that **C1**-sensitized cell outperforms **C2**- and **C3**-based devices, in terms of both photocurrent and photopotential. Besides, it is interesting to highlight that these p-type DSSCs showed an outstanding stability when kept in our laboratory under ambient light and temperature for 50 days. As shown in **Figure 4(b)**, all the cells were able to keep their initial efficiency in the aging test; surprisingly, **C1**- and **C3**-sensitized devices also improved their performance in the first month, probably due to the optimization of electrode wetting by the electrolyte solution and the formation of a stable photoelectrode-electrolyte interface. The outcome of this aging test is truly interesting, especially if we consider the very few works in the literature where stability tests on p-DSSC architectures are reported [29]. These results motivates further studies on the optical and photo-electrochemical properties of the C1-C3 based photocathodes and of the p-DSSC devices with more refined experimental characterization that we planned for a next future work.

Table 3. Comparison of the main photovoltaic parameters obtained from the J–V curves of the p-DSSCs with differently sensitized NiO electrodes.

	V_{oc} (mV)		J_{sc} (mA cm^{-2})		FF (%)		PCE (%)	
	1d	50d	1d	50d	1d	50d	1d	50d
C1	132	141	0.942	0.946	37.0	37.0	0.046	0.049
C2	104	118	0.380	0.280	44.8	51.7	0.018	0.017
C3	93	132	0.620	0.590	35.2	34.4	0.020	0.027
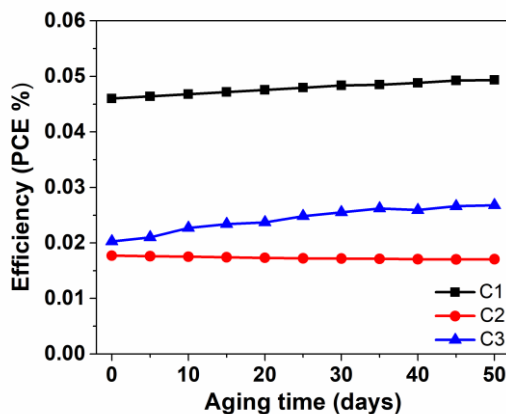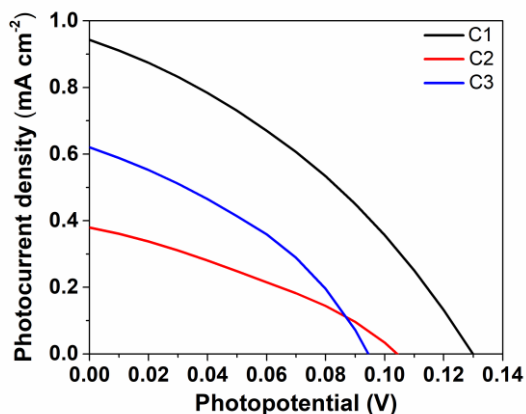
Figure 4. (A) Characteristic J−V curves of the NiO-based p-DSSCs with **C1**, **C2** and **C3** sensitizers. (B) PCE *vs.* aging time under ambient temperature/light for NiO-based p-DSSCs with **C1**, **C2** and **C3** sensitizers.

3. CONCLUSIONS

In this work we have presented three novel push-pull dyes, based on the same carbazole core and three different electron acceptor groups. We have characterized the optical, thermal and electrochemical properties of these dyes.

Beside, we have performed a theoretical analysis based on DFT and TD-DFT in order to dissect the properties of the dye and the dye-electrode interface that can both play a crucial role in the PCE performances of the p-DSSCs. From analysis of molecular properties (vertical electronic excitation, ICT parameters) and interfacial features (hole-injection driving force and charge recombination probability) we found the following relevant conclusions.

- The dye optical properties show that the C3 has the most effective electron withdrawing group, as expected.

- The **C1** dye has the largest driving force for hole injection in the dye-electrode interface calculations (-0.73 eV). The **C2** and **C3** dyes have similar but lower driving force (~-0.5 eV). It is worth mentioning that the electrochemical characterization of isolated dyes in solution provided a different qualitative picture, with all the three dyes with absolute HOMO energies within ~0.05 eV.

- For each of the three dyes, the distance between the dye LUMO (where the excited electron is localized) and the NiO surface is around ~10Å, no qualitative differences were found among **C1**, **C2** and **C3**. Hence, all the three dyes present the same probability for charge recombination, which should be low as expected by the good localization of the LUMO far from the NiO surface.

Eventually we have implemented the three new dyes into p-type DSSC devices with the standard NiO-based p-type semiconducting electrode. These cells provided a maximum PCE of ~0.05% for the **C1** dye, the trend of performances being **C1** > **C3** > **C2**. Overall the obtained conversion efficiencies are of the same order of magnitude of reference push-pull dyes such as the **P1**. However, it is worth mentioning that the p-DSSCs have showed a remarkable resistance to aging and the PCE measured after 50 days of storage at room temperature were actually better than the first tests. These preliminary results confirm the observations derived from the analysis of molecular and interfacial electronic properties and pave the route toward further characterization of p-DSSC technologies based on carbazole-derived push-pull dyes.

4. EXPERIMENTAL SECTION

General

All compounds were characterized by standard techniques. ^{1}H NMR and ^{13}C NMR spectra were recorded on Bruker Avance 400 MHz or Varian Inova 500 MHz spectrometers. DSC analyses were performed in dry ultrapure nitrogen flow using a Pyris 1 PerkinElmer apparatus at a scan rate of 10 K/min. Thermogravimetric analysis (TGA) were performed in air flow using a TA4000 PerkinElmer apparatus at a scan rate of 20 K min^{-1}. UV-Vis spectra of THF solutions of the dyes were recorded on a spectrophotometer Jasco V-560 (scan rate 200 nm min^{-1}). FTIR spectra of the dyes dispersed in KBr pellets were recorded on a FTIR Jasco F-430 spectrophotometer. Matrix-assisted laser desorption/ionization was performed on Bruker Solarix XR spectrometer using DHB as matrix.

Dye synthesis

All reagent and solvents were purchased from Sigma Aldrich and were used without further purification. 9-hexyl-9H-carbazole (**1**), 9-hexyl-9H-carbazole-3-carbaldehyde (**2**), 6-bromo-9-hexyl-

Synthesis of (Z)-3-(6-formyl-9-hexyl-9H-carbazol-3-yl)acrylic acid (**4**)

Compound **3** (3.000 g, 0.0086 mol) and acrylic acid (3.10 g, 0.043 mol) were dissolved in 15 mL of dry DMF; the solution was degassed with nitrogen for 15 min and then palladium acetate (0.43 mmol, 96 mg), tri-o-tolylphosphine (0.262 g, 0.86 mmol) and triethylamine (3 mL, 2.17 g, 0.0215 mol) were added. The system was kept at 90°C for 18 h, stirred under nitrogen. The reaction mixture was then cooled down to ambient temperature and poured in 200 mL of water + 10 mL HCl conc., at 0°C. A yellow solid formed that was recovered by filtration. The compound was then treated with 100 mL of chloroform and the insoluble part was filtered off; the chloroform solution was washed with brine and water, dried over Na_2SO_4 and the solvent removed at reduced pressure. A yellow solid was obtained that was then used for the following reaction without further purification. The yield was 65%.

^{1}H-NMR (DMSO-d6, 400 MHz): δ= 0.79 (t, 3H, J=6.8 Hz); 1.21-1.26 (m, 6H); 1.76 (m, 2H); 4.46 (d, 2H, J=6.8 Hz); 6.62 (d, 1H, J=16.0 Hz); 7.71 (d, 1H, J=8.4 Hz); 7.78 -7.81 (m, 2H); 7.87 (d, 1H, J=8.4 Hz); 8.70 (s, 1H); 8.81(s, 1H); 9.78 (s, 1H).

^{13}C-NMR (100MHz, CDCl3) δ= 14.22; 22.40; 26.42; 28.88; 31.32; 45.84; 109.12; 110.51; 113.21; 121.64; 123.52; 124.31; 124.55; 127.11; 128.44; 129.51; 139.92; 144.51; 190.42.

Synthesis of (E)-3-(6-(2,2-dicyanovinyl)-9-hexyl-9H-carbazol-3-yl)acrylic acid (**C1**)

Compound **4** (0.300 g, 0.860 mmol) and malononitrile (0.068 g, 1.03 mmol) were suspended in 6 mL of dry toluene, under nitrogen atmosphere. 50 mg of 3-aminopropyl functionalized silica gel (≈1.0 mmol g^{-1} NH$_2$ loading) were added and the system was taken at reflux to allow the solubilization of the reagents. During the reaction the formation of a yellow solid occurred. The system was kept at reflux overnight. The yellow solid was recovered by filtration, solved in 50 mL of THF and re-filtered to remove all the inorganic particles. The product was finally recrystallized by acetonitrile. The final yield was 70%.

M.p.: 242°C.

^{1}H-NMR (THF-d8, 400 MHz): δ= 0.86 (t, 3H, J=7.1 Hz); 1.30-1.42 (m, 6H); 1.89 (m, 2H); 4.43 (d, 2H, J=7.3 Hz); 6.52 (d, 1H, J=15.9 Hz); 7.61 (d, 1H, J=8.6 Hz); 7.69 (d, 1H, J=8.8 Hz); 7.81-7.86 (m, 2H); 8.19 (s, 1H); 8.23 (dd, 1H, J1=8.0 Hz; J2=1.6 Hz); 8.36 (s, 1H); 8.69 (d, 1H, J=1.6 Hz).

^{13}C-NMR (THF-d8, 400 MHz): δ= 13.33, 22.44, 28.69, 28.88, 31.50, 43.18, 76.96, 110.21, 113.97, 114.70, 116.79, 121.13, 123.01, 123.35, 123.45, 125.36, 126.68, 127.90, 127.94, 142.26, 144.14, 144.46, 160.00, 167.02.

HRMS m/z calcd. for $C_{25}H_{23}N_3O_2$: 397.1785; found: 397.1786, [M]$^+$

FT-IR (KBr pellets): ν (cm^{-1}): 2929, 2221, 1691, 1624, 1596, 1562, 1482, 1393, 1310, 1240, 1213, 1133, 977, 811, 641.

<u>Synthesis of (E)-3-(6-((1,3-diethyl-4,6-dioxo-2-thioxotetrahydropyrimidin-5(2H)-ylidene)methyl)-9-hexyl-9H-carbazol-3-yl)acrylic acid</u> (**C2**)

Compound **4** (0.300 g, 0.860 mmol) and N,N-diethyl-thiobarbituric acid (0.206 g, 1.03 mmol) were suspended in 6 mL of dry toluene, under nitrogen atmosphere. 50 mg of 3-aminopropyl functionalized silica gel (≈1.0 mmol/g NH$_2$ loading) were added and the system was taken at reflux to allow the solubilization of the reagents. During the reaction the formation of a yellow solid occurred. The system was kept at reflux overnight. The yellow solid was recovered by filtration, solved in 50 mL of THF and re-filtered to remove all the inorganic particles. The product was finally recrystallized by THF/ethanol. The final yield was 74%.

M.p.: 263°C

^{1}H-NMR (THF-d8, 400 MHz): δ= 0.87 (t, 3H, J=7.0 Hz); 1.33-1.46 (m, 12H); 1.91 (m, 2H); 4.44 (t, 2H, J=6.8 Hz); 4.58-4.63 (m, 4H); 6.54 (d, 1H, J=16.0 Hz); 7.61 (d, 2H, J=8.4 Hz); 7.81 (d, 1H, J=8.4 Hz); 7.87 (d, 1H, J=16.0 Hz)); 8.44 (s, 1H); 8.65 (d, 1H, J=8.8 Hz)); 8.73 (s, 1H); 9.46 (s, 1H); 10.83 (s, 1H).

^{13}C-NMR (THF-d8, 400 MHz): δ= 11.73, 11.84, 13.33, 22.45, 26.70, 28.90, 31.52, 42.96, 43.14, 43.51, 109.03, 110.04, 114.81, 116.58, 121.11, 123.14, 123.66, 125.05, 126.36, 127.83, 129.96, 134.60, 142.30, 144.46, 144.63, 158.92, 159.64, 161.22, 167.00, 179.24

HRMS m/z calcd. for $C_{30}H_{34}N_3O_4S$: 532.2264, found: 532.2271, [MH$^+$].

FT-IR (KBr pellets): ν (cm^{-1}): 2929, 1683, 1660, 1621, 1525, 1486, 1462, 1415, 1385, 1285, 1244, 1206, 1158, 1096, 1074, 806, 783.

Synthesis of (E)-3-(6-((Z)-(1-(dicyanomethylene)-3-oxo-1H-inden-2(3H)-ylidene)methyl)-9-hexyl-9H-carbazol-3-yl)acrylic acid (C3)

Compound **4** (0.300 g, 0.860 mmol) and 1,3-diethyl-2-thioxodihydropyrimidine-4,6(1H,5H)-dione (0.200 g, 1.03 mmol) were suspended in 6 mL of dry toluene, under nitrogen atmosphere. 50 mg of 3-aminopropyl functionalized silica gel (≈1.0 mmol g^{-1} NH$_2$ loading) were added and the system was taken at reflux to allow the solubilization of the reagents. During the reaction the formation of a yellow solid occurred. The system was kept at reflux overnight. The yellow solid was recovered by filtration, solved in 50 mL of THF and re-filtered to remove all the inorganic particles. The product was finally recrystallized by THF/ethanol. The final yield was 65%.

M.p.: 278°C

^{1}H-NMR (THF-d8, 400 MHz): δ= 0.87 (t, 3H, J=6.9 Hz); 1.33-1.46 (m, 6H); 1.89-1.93 (m, 2H); 4.44 (t, 2H, J=7.2 Hz); 6.56 (d, 1H, J=16.0 Hz); 7.60 (d, 1H, J=8.8 Hz); 7.64 (d, 1H, J=8.8 Hz); 7.78-7.88 (m; 4H); 7.94 (d, 1H, J=6.8 Hz); 8.49 (s, 1H); 8.57 (d, 1H, J=7.6 Hz); 8.67 (d, 1H, J=7.2 Hz); 8.80 (s, 1H); 9.33 (s, 1H), 10.83 (s, 1H).

^{13}C-NMR (THF-d8, 400 MHz): δ= 13.34, 26.69, 28.91, 31.53, 43.16, 70.28, 109.37, 110.04, 114.30, 114.59, 116.63, 121.08, 123.38, 123.57, 124.61, 125.14, 126.53, 126.64, 127.91, 128.92, 133.69, 134.35, 134.85, 139.77, 142.28, 144.37, 144.60, 148.11, 162.35, 137.02, 186.30.

HRMS m/z calcd. for calcd. for $C_{34}H_{28}N_3O_3$: 526.2125, found: 526.2120, [MH$^+$].

FT-IR (KBr pellets): ν (cm^{-1}): 2924, 2212, 1677, 1528, 1460, 1412, 1383, 1343, 1237, 1206, 1158, 986, 807, 719.

Electrochemical characterization

Electrochemical measurements were performed with a Metrohm 757 VA Computrace combined with an AUTOLAB potentiostat-galvanostat. Voltammetric experiments were run under argon on dichloromethane solution (≈0.5 mM) of the dyes; the scan was performed at room temperature at 100 mV s^{-1} rate. A single compartment three-electrode cell was employed, with a platinum carbon working electrode, platinum wire as counter electrode and Ag/AgCl as reference electrode (all purchased from Tokai Electrode Manufacturing Co.); Ferrocene/Ferrocenium (Fc/Fc^{+}, Sigma-Aldrich) redox couple was used as internal reference. Tetrabutylammonium hexafluorophosphate (100 mM) served as non-redox electrolyte.

Computational details

First-principles calculations at the DFT and TD-DFT levels of theory were performed in order to investigate the dye molecular properties and the dye-electrode interfacial features. We used the Gaussian09 program [56] for the characterization of the dyes and the VASP code [57] for the dye-NiO interface. Ground-state minimum energy structures, vibrational frequencies and molecular orbital energy levels of dye molecules were computed with the PBE0 exchange-correlation functional [58], while the long-range corrected CAM-B3LYP density functional [59] was used to predict the dye excited state properties (i.e. absorption energies as well as 0-0 transitions). The TZVP basis set [60] was used for C, N, O, H and S atoms. All the calculations were performed in acetonitrile (ε_{ACN}=35.688) described by the PCM implicit solvation scheme [32]. Moreover, we analysed the extent of the intramolecular charge transfer upon excitation by means of charge transfer indexes as recently proposed by Le Bahers *et al*. [49].

The dye-NiO interface was investigated by means of a vacuum slab periodic approach, exploiting the rotationally invariant DFT+U approach as implemented in VASP [61]. We applied the Perdew-

Burke-Ernzerohof (PBE) exchange-correlation density functional [62], plus a U-J term of 3.8 eV for Ni d states, as derived by the ab initio DFT+U scheme [63,64]. The p-type character of NiO was modelled by removing a neutral Ni atom from the 3x3 5 - layer slab. The so obtained concentration of holes is a lot higher than typical hole concentrations in real systems. However, to reproduce the correct doping percentage we would need a huge supercell which would make the calculation completely unaffordable. Solvent effects at the interface were also included by means of a PCM-like implicit solvation scheme as implemented in the VASP_sol code [49]. Projector-augmented wave (PAW) potentials were used for treating nuclei and core electrons, [65] while valence electrons were expanded in a plane wave basis set with a 600 eV cut-off. For the vacuum slab, we exploited a 3x3x1 Γ-centered k-point mesh. All the exploited numerical parameters were recently validated in the case of C343/NiO interface [34].

DSSC fabrication and characterization

For the preparation of the NiO paste, all chemicals were purchased from Fluka or Merck at the highest degree of purity available and were used without any further purification [66]. 6 g of NiO nanopowder were grinded in a mortar with 1 mL of hydrochloric acid for 5 min, followed by the addition of 1 mL of distilled water and grinding for 1 min. This latter operation was repeated 5 times, reaching a final volume of 6 mL, followed by the addition of 1 mL of ethanol and grinding for 1 min. Ethanol was added 14 times more, resulting in a final volume of the mixture equal to 21 mL. In the following step, 2.5 mL of ethanol were added to the mixture and this operation was repeated 6 times (final volume: 36 mL). 100 mL of ethanol were used to transfer the paste into a beaker, where it was stirred for 1 min, sonicated for 2 min and stirred again for 1 min. 20 g of anhydrous terpineol (as a mixture of enantiomers) were added to the mixture, then stirred for 1 min, sonicated for 2 min and stirred again for 1 min. A solution of ethyl cellulose (10 wt% in ethanol) was added to the mixture. We proceeded with 1 min of stirring, 2 min of sonication and 1 min more of stirring: this triple step was repeated 3 times. In order to allow the slow evaporation of the volatile components of the mixture, it was placed on a hot plate at 50°C for 9 h, and the cooled down to ambient temperature.

Fluorine-doped tin oxide (FTO) glass plates (sheet resistance, 7 Ω sq^{-1}, Solaronix) were cut into 2 cm × 2 cm sheets and used as substrates for the fabrication of NiO electrodes and platinized counter electrodes. A single layer of NiO was deposited on the top of the conductive FTO substrates (previously cleaned with acetone and ethanol) by a screen printer (AT-25PA, Atma Champ Ent. Comp) employing a 90.48 T mesh frame. After a pre-drying period of 15 min at 100°C in oven, the temperature of the oven was increased employing a temperature ramp of 15°C min^{-1} till 450 °C. After 30 min at 450°C, the mesoporous films of NiO were cooled down to ambient temperature and a thickness equal to 2 μm was measured by profilometry (P.10 KLA-Tencor Profiler). Sensitization of screen-printed photocathodes (area = 0.20 cm^2) was carried out by dipping the electrodes film into a 0.2 mM solution of the dye-sensitizer in ethanol for 2 h. Concerning the counter electrode preparation, 5 nm Pt thin films were deposited by sputtering (Q150 T ES, Quorum Technologies Ltd) onto cleaned FTO glasses [67-69].

Finally, the two electrodes were irreversibly sealed together by a thermoplastic spacer (Meltonix 1170-25/PF, 50 μm thick, Solaronix) and hot-pressed under mild pressure at 90°C. The sandwiched cells were filled with the electrolyte (Iodolyte Z-150, Solaronix) by a vacuum procedure. The inlet was finally sealed by a thermoplastic sheet in a combination with a small glass cap [68,69] Photocurrent–photovoltage (J–V) curves were measured using a Keithley 2440 Source Measure Unit under AM 1.5G illumination (100 mW cm^{-2}) provided by a Newport 91195A class A solar simulator (calibrated through a Newport 91150 V silicon reference solar cell) [72,73]. The active area of the cells was defined as 0.16 cm^2 using a black mask.

ACKNOWLEDGMENTS

REFERENCES

[1] A. Kirubakaran, S. Jain, R. K. Nema, Renew. Sust. Energ. Rev., 13 (2009) 2430

[2] J. B. Goodenough, J Solid State Electrochem., 16 (2012) 2019

[3] N.L. Panwar, S. C. Kaushik, S. Kothari, Renew. Sust. Energ. Rev., 15 (2011) 1513

[4] M. A. Green, Prog. Photovolt: Res. Appl., 9 (2001) 123

[5] A. Hagfeldt, G. Boschloo, L. Sun, L. Kloo, H. Pettersson, Chem. Rev. 110 (2010) 6595

[6] B. O'Regan, M. Grätzel, Nature, 353 (1991) 737

[7] L. Kavan, Curr Opinion Electrochem., 2 (2017) 88

[8] M. M. Lee, J. Teuscher, T. Miyasaka, T. N. Murakami[2], H. J. Snaith, Science, 338 (2012) 643

[9] a) F. Würthner, K. Meerholz, Chem. Europ. J., 16 (2010) 9366; b) C. Maglione, A. Carella, R. Centore, P. Chávez, P. Lévêque, S. Fall, et al., Dyes Pigm., 141 (2017) 169

[10] A. Malafronte, F. Auriemma, R. Di Girolamo, C. Sasso, C. Diletto, A. E. Di Mauro, E. Fanizza, P. Morvillo, A. M. Rodriguez, A.B. Muñoz-Garcia, M. Pavone, C. De Rosa, J. Phys. Chem. C, 121 (2017) 16617

[11] D. Wang, M. Wright, N. K. Elumalai, A. Uddin, Sol. Energy Mat. Sol. Cells,147 (2016) 255

[12] K. Kakiage, Y. Aoyama, T. Yano, K. Oya, J-I. Fujisawa, M. Hanaya, Chem. Commun., 51 (2015) 15894

[13] S. Galliano, F. Bella, G. Piana, G. Giacona, G. Viscardi, C. Gerbaldi, M. Grätzel, C. Barolo, Sol. Energy, 163 (2018) 251

[14] S. Yoon, S. Tak, J. Kim, Y. Jun, K. Kang, J. Park Build Environ, 46 (2011) 1899

[15] M. Freitag, J. Teuscher, Y. Saygili, X. Zhang, F. Giordano, P. Liska, J. Hua, S. M. Zakeeruddin, J.E. Moser, M. Grätzel, A. Hagfeldt, Nat. Photonics, 11 (2017) 372

[16] A. Nattestad, A.J. Mozer, M. K. R. Fische, Y-B Cheng, A. Mishra, P. Bäuerle, U. Bach, Nat. Mater., 9 (2010) 31.

[17] D. Xiong, W. Chen, Front. Optoelectron., 5 (2012) 371

[18] W. Shockley, H.J. Queisser, J. Appl. Phys., 32 (1961) 510

[19] Y. Xu, T. Gong, J. N. Munday, Sci. Rep., 5 (2015) 13536

[20] I. Sullivan, B. Zoellner, P. A. Maggard, Chem. Mater., 28 (2016) 5999

[21] I. R. Perera, T. Daeneke, S. Makuta, Z. Yu, Y. Tachibana, A. Mishra, P. Bäuerle, C. A. Ohlin, U. Bach, L. Spiccia, Angew. Chemie, Int Ed 54 (2015) 3758

[22] L. D'Amario, G. Boschloo, A. Hagfeldt, L. Hammarström, J. Phys. Chem. C, 118 (2014) 19556

[23] T. Jiang, M. Bujoli-Doeuff, Y. Farré, Y. Pellegrin, E. Gautron, M. Boujtita, L. Cario, S. Jobic, F. Odobel, RSC Adv., 6 (2016) 112765

[24] L. D'Amario, L. J. Antila, B. R. Pettersson, G. Boschloo, L. Hammarström, J. Phys. Chem. Lett., 6 (2015) 779

[25] X. Li, F. Yu, S. Stappert, C. Li, Y. Zhou, Y. Yu, X. Li, H Ågren, J. Hua, H. Tian, ACS Appl. Mater. Interfaces, 8 (2016) 19393

[26] T. T. T. Pham, S. K. Saha, D. Provost, Y. Farré, M. Raissi, Y. Pellegrin, E. Blart, S. Vedraine, B. Ratier, D. Aldakov, F. Odobel, J. Bouclé, J. Phys. Chem. C, 121 (2017) 129 doi:10.1021/acs.jpcc.6b10513.

[27] Y. Farrè, L. Zhang, Y. Pellegrin, A. Planchat, E. Blart, M. Boujtita, L. Hammarström, D. Jacquemin, F. Odobel, J. Phys. Chem. C, 120 (2016) 7923

[28] J. Cui, J. Lu, X. Xu, K. Cao, Z. Wang, G. Alemu, H. Yuang, Y. Shen, J. Xu, Y. Cheng, M. Wang, J. Phys. Chem. C, 118 (2014) 16433

[29] Z. Liu, W. Li, S. Topa, X. Xu, X. Zeng, Z. Zhao, M. Wang, W. Chen, F. Wang, Y.-B. Cheng, H. He, ACS Appl. Mater. Interfaces, 6 (2014) 10614

[30] R. G. Parr, W. Yang, Density-Functional Theory of Atoms and Molecules. New York: Oxford University Press (1998)

[31] W. Kohn, L. J. Sham, Phys. Rev., 140 (1965) A1133

[32] E. Runge, E. K. U. Gross, Phys. Rev. Lett., 52 (1984) 997

[33] M. Cossi, V. Barone, R. Cammi, J. Tomasi, Chem. Phys. Lett., 255 (1996) 327

[34] A. B. Muñoz-García, M. Pavone, Phys. Chem. Chem. Phys., 17 (2015) 12238

[35] C. Maglione, A. Carella, C. Carbonara, R. Centore, S. Fusco, A. Velardo, A. Peluso, D. Colonna, A. Lanuti, A. Di Carlo, Dyes Pigm., 133 (2016) 395

[36] C. Maglione, A. Carella, R. Centore, S. Fusco, A. Velardo, A. Peluso, D. Colonna, A. Di Carlo, J. Photochem. Photobiol. A Chem., 321 (2016) 79

[37] A. Capobianco, A. Esposito, T. Caruso, F. Borbone, A. Carella, R. Centore, A. Peluso, Europ. J. Org. Chem. (2012) 2980

[38] P. Gautam, R. Maragani, R. Misra, Tetrahedron Lett., 55 (2014) 6827

[39] R. Misra, P. Gautam, S. M. Mobin, J. Org. Chem., 78 (2013) 12440

[40] B. List, Angew. Chemie Int. Ed., 49 (2010) 1730

[41] S. Galliano, V. Novelli, N. Barbero, A. Smarra, G. Viscardi, R. Borrelli, F. Sauvage C. Barolo, Energies, 9 (2016) 486

[42] L. Muralidhar, C. R. Girija, J. Saudi. Chem. Soc. 18 (2014) 541

[43] R. Menegatti, Green Chemistry – Aspects for the Knoevenagel Reaction. Green Chem. Environ. Benign Approaches, InTech (2012) doi:10.5772/36489.

[44] X. M. Hu, Y. Zhao, Y. F. Gao, Y. B. Xiao, B. X. Zhang, Adv. Mater. Res. 554-556 (2012) 557

[45] E. Angeletti, C. Canepa, G. Martinetti, P. Venturello, J. Chem. Soc. Perkin Trans. 1 (1989)

[46] D. J. Macquarrie, J. H. Clark, A. Lambert, J. E. Mdoe, A. Priest, React. Funct. Polym., 35 (1997) 153

[47] H. Krysova, J. Barton, V. Petrak, R. Jurok, M. Kuchar, P. Cigler, L. Kavan Phys. Chem. Chem. Phys. 18 (2016) 16444-16450

[48] C. M. Cardona, W. Li, A. E. Kaifer, D. Stockdale, G. C. Bazan, Adv. Mater., 23 (2011) 2367

[49] T. Le Bahers, C. Adamo, I. Ciofini, J. Chem. Theory Comput., 8 (2011) 2498

[50] J.N. Clifford, E. Palomares, M.K Nazeeruddin, M. Grätzel, J. Nelson, X. Li, N.J. Long, J. R. Durrant, J. Am. Chem. Soc. 126 (2004) 5225

[51] a) J. Z. Zhang, J. Zhang, H.-B. Li, Y. Wou, H.-L. Xu, M. Zhang, Y. Geng, Zhong-Min Su. Journal of Power Sources 267 (2014) 300 b) J. Feng, Y. Jiao, W. Ma, Md. K. Nazeeruddin, M. Grätzel, S. Meng. J. Phys. Chem. C, 117 (2013) 3772

[52] S. Karamshuk, S. Caramori, N. Manfredi, M. Salamone, R. Ruffo, S. Carli, C. A. Bignozzi, C.A. Abbotto, Energies, 9 (2016) 33

[53] M. Bonomo, A. Carella, R. Centore, A. Di Carlo, D. Dini, J. Electrochem. Soc. 164 (2017) F1412

[54] P. Naik, A. Planchat, Y. Pellegrin, F. Odobel, A. V. Adhikari, Sol. Energy, 157 (2017) 1064

[55] M.-J. Cho, J.-Y Kim, J.-H. Kim,S. –H. Lee, L. R. Dalton, D.-H. Choi, Bulletin of the Korean Chemical Society, 26 (2005) 77

[56] Frisch M. J., Trucks G. W., Schlegel H. B., Scuseria G. E., Robb M. A., Cheeseman J. R., Scalmani G., Barone V., Mennucci B., Petersson G. A., Nakatsuji H., Caricato M., Li X., Hratchian H. P., Izmaylov A. F., Bloino J., Zheng G., Sonnenberg J. L., Hada M., Ehara M., Toyota K., Fukuda R., Hasegawa J., Ishida M., Nakajima T., Honda Y., Kitao O., Nakai H., Vreven T., Montgomery J. A. Jr., Peralta J. E., Ogliaro F., Bearpark M., Heyd J. J., Brothers E., Kudin K. N., Staroverov V. N., Kobayashi R., Normand J., Raghavachari K., Rendell A., Burant J. C., Iyengar S. S., Tomasi J., Cossi M., Rega N., Millam J. M., Klene M., Knox J. E., Cross J. B., Bakken V., Adamo C., Jaramillo J., Gomperts R., Stratmann R. E., Yazyev O., Austin A. J., Cammi R., Pomelli C., Ochterski J. W., Martin R. L., Morokuma K., Zakrzewski V. G., Voth G. A., Salvador P., Dannenberg J. J., Dapprich S., Daniels A. D., Farkas O., Foresman J. B., Ortiz J. V., Cioslowski J., Fox D. J., Gaussian 09, revision E.01, Gaussian Inc.: Wallingford, CT (2009)

[57] (a) G. Kresse, J. Furthmüller, Comp. Mat. Sci., 6 (1996) 15; (b) G. Kresse, J. Furthmüller, Phys. Rev. B, 54 (1996) 11169; (c) K. Mathew, R. Sundararaman, K. Lerchworth-Weaver, T.A. Arias, R. G. Henning, J. Chem. Phys. 140 (2014) 084106

[58] C. Adamo, V. Barone, J. Chem. Phys., 110 (1999) 6158

[59] T. Yanai, D. P. Tew, N. C. Handy, Chem. Phys. Lett., 393, (2004) 51

[60] N. Godbout, D. R. Salahub, J. Andzelm, and E. Wimmer, Can. J. Chem., 70 (1992) 560

[61] S. L. Dudarev, G. A. Botton, S. Y. Savrasov, C. J. Humphreys, A. P. Sutton, Phys. Rev. B 57(1998) 1505

[62] J. P. Perdew, K. Burke, M. Ernzerhof, PRL 77 (1996) 3865

[63] (a) N. Alidoust, M. C. Toroker, J. A. Keith and E. A. Carter, Chem. Sus. Chem., 7 (2014) 195; (b) N. Alidoust, M. C. Toroker and E. A. Carter, J. Phys. Chem. B, 118 (2014) 7963

[64] N. J. Mosey, E. A. Carter, Phys. Rev. B, 76 (2007) 155123

[65] P.E. Blöchl, Phys Rev. B, 24 (1994) 17953

[66] M. Bonomo, N. Barbero, F. Matteocci, A. D. Carlo, C. Barolo, D. Dini, J. Phys. Chem. C, 120 (2016) 16340

[67] G. Yang, Y. Tang, X. Li, H. Ågren, Y. Xie, ACS Appl. Mater. Interfaces, 9 (2017) 36875

[68] S. B. Akula, H.-S. Chen, C. Su, C.-R. Chen, J.-J. Chiou, C.-H. Shieh, Y.-F. Lin, W.-R. Li, Inorg. Chem., 56 (2017) 12987

[69] Z. Hosseini, N. Taghavinia, E. Wei-Guang Diau, Chem. Phys. Chem., 18 (2017) 3292

[70] F. Bella, J. Popovic, A. Lamberti, E. Tresso, C. Gerbaldi, J. Maier, ACS Appl. Mater. Interfaces, 9 (2017) 37797

[71] F. Bella, A. Verna, C. Gerbaldi, Mater. Sci. Semicon. Process., 73(2018). 92

[72] L. J. Brennan, F. Purcell-Milton, B. McKenna, T. M. Watson, Y. K. Gun'ko, R. C. Evans, J. Mater. Chem. A, 6 (2018) 2671

[73] S. Venkatesan, E. S. Darlim, I.-P. Liu, Y.-L Lee, Carbon, 132 (2018) 71

[74] G. Ponti, F. Palombi, D. Abate, F. Ambrosino, G. Aprea, T. Bastianelli, F. Beone, R. Bertini, G. Bracco, M. Caporicci, B. Calosso, M. Chinnici, A. Colavincenzo, A. Cucurullo, M. De Rosa, P. De Michele, A. Funel, G. Furini, D. Giammattei, S. Giusepponi, R. Guadagni, G. Guarnieri, A. Italiano, S. Magagnino, A. Mariano, G. Mencuccini, C. Mercuri, S. Migliori, P. Ornelli, S. Pecoraro, A. Perozziello, S. Pierattini, S. Podda, F. Poggi, A. Quintiliani, A. Rocchi, C. Scio', F. Simoni, A. Vita *The role of medium size facilities in the HPC ecosystem: the case of the new CRESCO4 cluster integrated in the ENEAGRID infrastructure.* Proceedings of the 2014 International Conference on High Performance Computing and Simulation (HPCS); IEEE, 2014; Article 6903807, pp 1030−1033.

Supplementary Materials